1.55-μm AlGaInAs/InP Sampled Grating Laser Diodes for Mode Locking at Terahertz Frequencies

Lianping Hou, *Member, IEEE*, Song Tang, Bin Hou, Song Liang, and John H. Marsh, *Fellow, IEEE*

***Abstract*—We report mode locking in lasers integrated with semiconductor optical amplifiers, using either conventional or phase-shifted sampled grating distributed Bragg reflectors (DBRs). For conventional sampled gratings with a continuous grating coupling coefficient of $\sim$80 cm^{-1}, mode locking was observed at a fundamental frequency of 628 GHz and second harmonic of 1.20 THz. The peak output power was up to 142 mW. In the phase-shifted sampled grating design, the grating is present along the entire length of the reflector with π-phase-shifted steps within each sampled section. The effective coupling coefficient is, therefore, increased substantially. Although the continuous grating coupling coefficient for the phase-shifted gratings was reduced to $\sim$23 cm^{-1} because of a different fabrication technology, the lasers demonstrated mode locking at fundamental repetition frequencies of 620 GHz and 1 THz, with a much lower level of amplified spontaneous emission seen in the output spectra than from conventional sampled grating devices. High pulse reproducibility and controllability over a wide operation range was seen for both types of grating, but the π-phase-shifted gratings already demonstrate fundamental mode locking to 1 THz. The integrated semiconductor optical amplifier makes sampled grating DBR lasers ideal pump sources for generating terahertz signals through photomixing.**

***Index Terms*—Semiconductor lasers, distributed Bragg reflector lasers, mode locked lasers.**

I. Introduction

ULTRAFAST mode-locked laser diodes (MLLDs) offer exciting opportunities in future telecoms systems, high speed data processing and miniaturized THz signal generators because they are compact, robust, cheap to manufacture, and can be integrated with other semiconductor elements such as semiconductor optical amplifiers (SOAs). Mode-locking is a well-established route for generating short pulses, and the short cavity length of semiconductor lasers also offers high repetition frequencies (a 500 μm cavity corresponds to a round-trip frequency of $\sim$80 GHz). A robust solution for generating still higher frequency pulse streams is to utilize harmonic mode-locking (HML) techniques, with compound-cavity mode-locking (CCM) [1], [2] and colliding pulse mode-locking (CPM) [3] widely reported (for a recent review, see [4]).

To overcome the disadvantages of CPM and CCM lasers, we have previously proposed the use of sampled grating distributed Bragg reflector (DBR) lasers for reaching sub-THz repetition frequencies [5]. These DBR lasers make use of conventional sampled-gratings (C-SGDBR), with grating sections spaced apart by sections of waveguide with no grating. Devices based on C-SGDBRs have been shown to offer far superior reproducibility, controllability, and a wider operation range than all other reported types of THz repetition frequency MLLDs [4], [5]. This class of device therefore represents a significant advancement in the HML field.

A significant disadvantage of a C-SGDBR is that the effective coupling coefficient, κ, is reduced substantially from that of a uniform grating, largely because much of the sampling period has no grating. The use of π-phase shifted (PPS) SGDBRs (PPS-SGDBRs) can overcome this limitation, as we have demonstrated in cw semiconductor lasers [6].

In this paper, we report the use of monolithically integrated SOAs to increase the average output power of sub-THz and THz mode-locked pulse trains. Integrated SOAs allow the average power and peak power to be increased to more than 50 mW and 140 mW respectively. We also report mode-locking in PPS-SGDBR lasers and compare C-SGDBR and PPS-SGDBR MLLDs directly. Compared with the C-SGDBR, the PPS-SGDBR has significantly larger coupling between the optical field and the grating, so the number of grating periods and the total length of monolithic SGDBR lasers can be reduced. The higher coupling also enables shorter periods of the sampled grating to be used, allowing higher mode-locked frequencies to be realized.

To the best of our knowledge, these are the first reports of such constructions, and because of the good mode control and high output power, these devices can be used directly as pump sources for THz signal production using photomixing techniques [7], without the need for additional amplification using, for example, erbium-doped fiber amplifiers (EDFAs).

In Section II, the configurations of C-SGDBR and PPS-SGDBR lasers will be compared. In Section III, the epitaxial structures and fabrication techniques are described. We will then describe the performance of C-SGDBRs integrated with an SOA in Section IV and the novel PPS-SGDBR integrated with an SOA in Section V.

Manuscript received January 29, 2018; revised March 27, 2018; accepted April 11, 2018. Date of publication April 20, 2018; date of current version May 8, 2018. This work was supported in part by the U.K. Engineering and Physical Sciences Research Council under Grant EP/E065112/1 and in part by the National Science Foundation of China under Grant 61320106013. *(Corresponding author: Lianping Hou.)*

L. Hou, S. Tang, B. Hou, and J. H. Marsh are with the School of Engineering, University of Glasgow, Glasgow G12 8QQ, U.K. (e-mail: lianping.hou@glasgow.ac.uk; s.tang.1@research.gla.ac.uk; b.hou.1@research.gla.ac.uk; john.marsh@glasgow.ac.uk).

S. Liang is with the Institute of Semiconductors, Chinese Academy of Sciences, Beijing 100083, China (e-mail: liangsong@semi.ac.cn).

Color versions of one or more of the figures in this paper are available online at http://ieeexplore.ieee.org.

Digital Object Identifier 10.1109/JSTQE.2018.2827672

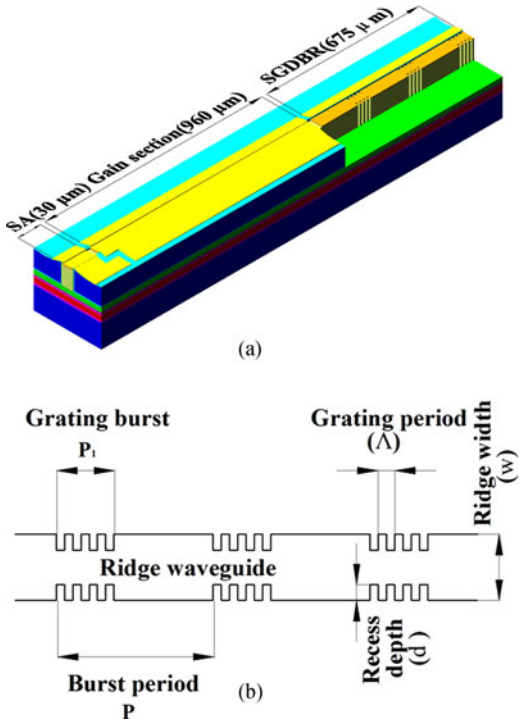

Fig. 1. (a) Schematic of the MLLD based on C-SGDBR, (b) configuration of the first-order sidewall C-SGDBR with a 0.6 μm recess (d).

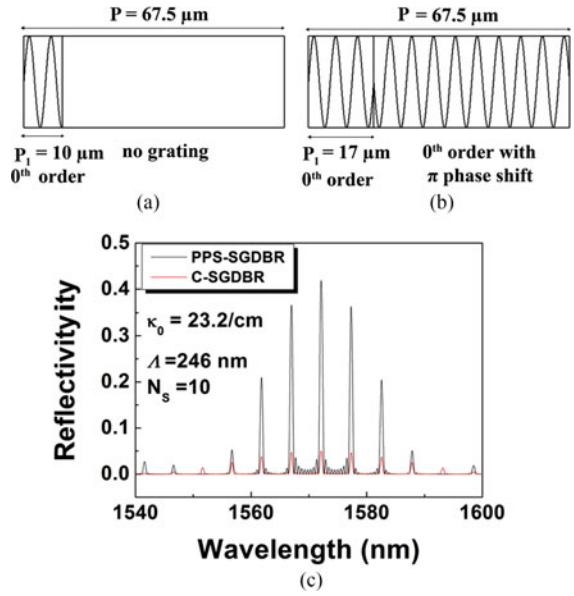

Fig. 2. Device structures based on (a) C-SGDBR, (b) PPS-SGDBR, and (c) simulated reflection spectra for C-SGDBR and PPS-SGDBR.

II. Side-Wall C-SGDBR and PPS-SGDBR Configurations

The SGDBR laser has been reported previously [4], [5] and, as shown in Fig. 1(a), consists of a reflecting facet, a saturable absorber (SA), a gain section and a SGDBR reflector. Their advantages for HML include:

- The SGDBR accurately determines the wavelength of operation and acts as a filter, providing strong selection of the modes desired for HML.
- Pulses are reflected into the main cavity from the DBR, and the laser self-adjusts so that the spectral resonances of the SGDBR align with a sub-set of the resonant frequencies of the main cavity.
- The SGDBR concept relaxes the stringent fabrication and cleaving tolerances associated with other HML constructions (CPM and CCM), so devices can be fabricated as readily as conventional ridge waveguide lasers.

The gratings of the C-SGDBR MLLD are etched into the side-walls of a ridge waveguide as shown in in Fig. 1(b) [4], [5]. The mode-locked frequency is set by the round trip time of one period of the sampled grating (P):

$$F_r = c/(2n_g P) \tag{1}$$

where c is the velocity of light in free space, and n_g is the group index, $\approx$3.4889. P represents the burst period of the grating and has a value of 67.5 μm for a mode-locking frequency of 640 GHz. P_1 represents the length of the grating burst, which is 10 μm long and of first-order with a 50% duty cycle and formed by etching 0.6 μm deep recesses (d) into the sidewalls of the waveguide. Λ represents the grating period and is 245 nm. The coupling coefficient of a uniform grating, κ_0, was measured to be approximately 80 cm^{-1} when using a reactive-ion etching (RIE) machine with an optimized dry etch recipe [4], [5].

Fig. 2 illustrates a C-SGDBR and a PPS-SGDBR. The C-SGDBR structure is the same as that of Fig. 1, except here the grating period $\Lambda = 246$ nm and $\kappa_0 = 23.2$ cm^{-1}. The number of sampling periods N_s is 10. When the duty cycle of the PPS-SGDBR is chosen to be $P_1/P = 0.25$, the different order peaks in the reflection spectrum are most uniform which is suitable for the THz repetition frequency mode locking. The effective κ of the PPS-SGDBR is expected to be more than three times $((67.5 - 2 \times 17)/10 = 3.35)$ that of a C-SGDBR and nearly half $((67.5 - 2 \times 17)/67.5 = 0.4963)$ that of a uniform grating. The 0$^{\text{th}}$ order gratings have a period of 246 nm, sampling period $P = 67.5\,\mu$m, and the grating burst $P_1 = 10\,\mu$m and 17 μm for the C-SGDBR and PPS-SGDBR respectively. Transfer matrix simulations of the reflectivity of the two kinds of SGDBR confirm this analysis (Fig. 2(c)). The central peak wavelength (λ_{peak}) is 1572 nm and the spacing between reflectivity peaks is about 5.22 nm. Here we ran the grating dry etch process in a new inductively coupled plasma (ICP) machine which is not yet fully optimized. The recipe we used resulted in a rougher grating surface and exhibited a RIE lag effect, so here the coupling coefficient of a uniform grating, κ_0, was measured to be approximately 23.2 cm^{-1}, less than that of 80 cm^{-1} using the optimized RIE dry etch recipe.

III. Material Structure and Fabrication

In the work reported here, we used a five quantum well (QW) AlGaInAs/InP structure grown in a single step which has been described in our previous research [8]. We use a side-wall etched SGDBR which can be simultaneously defined and fabricated

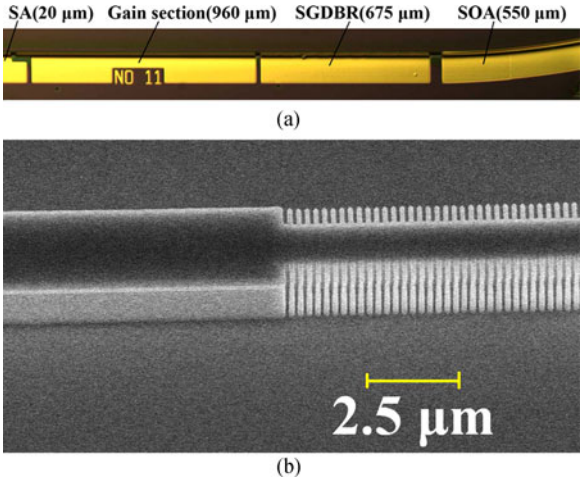

Fig. 3. (a) Optical microscope picture of the MLLD integrated with an SOA, (b) the SEM picture of the side-wall grating burst of first-order with a 50% duty cycle and 0.6 μm depth recesses.

along with the ridge waveguide using conventional electron beam lithography (EBL) and RIE (ICP) techniques, eliminating the oxidation of the active layer and the need for overgrowth and simplifying the fabrication process [9]. The device fabrication procedures were similar to those described in [10], and the lasers were tested under CW biasing conditions at 20 °C. Here we need to point out that the C-SGDBR MLLD described in Section IV was fabricated using an old RIE machine with an optimized dry etch recipe and the PPS-SGDBR and its counterpart C-SGDBR in Section V were fabricated using a new ICP machine which is not yet fully optimized. As a result, the continuous grating κ_0 was reduced for the new process. Both facets were uncoated, but the angled waveguide at the SOA side of the device minimizes back-reflections from the output facet [11].

IV. C-SGDBR MLLD Integrated With an SOA

An optical microscope picture of the top view (p-side) of the fabricated device of the C-SGDBR MLLD integrated with a SOA along with its dimensions is shown in Fig. 3(a). For simplicity, we shall refer to the C-SGDBR as the SGDBR in this section. The device has a total length of 2295 μm of which the gain section is 960 μm, the saturable absorber (SA) section is 20 μm, and the SGDBR section is 675 μm. The ridge waveguide width (w) for these sections is 2.5 μm. The curved SOA is 550 μm long, with w increasing from 2.5 μm to 6 μm with a curvature radius of 3455 μm. This results in a tilt of 10° at the output facet to reduce the optical reflectivity [11]. The electrical isolation gap between the SA, gain and SGDBR sections is 20 μm, and the gap between the SOA and SGDBR sections is 50 μm. The configuration of the SGDBR section is the same as that in Fig. 1(b), and an SEM picture of the side-wall grating burst of first-order with a 50% duty cycle and 0.6 μm depth recesses is shown in Fig. 3(b). As discussed in Section II, for these devices the coupling coefficient of a uniform grating, κ_0, was measured to be approximately 80 cm^{-1} using the sub-threshold spectral fitting method [12].

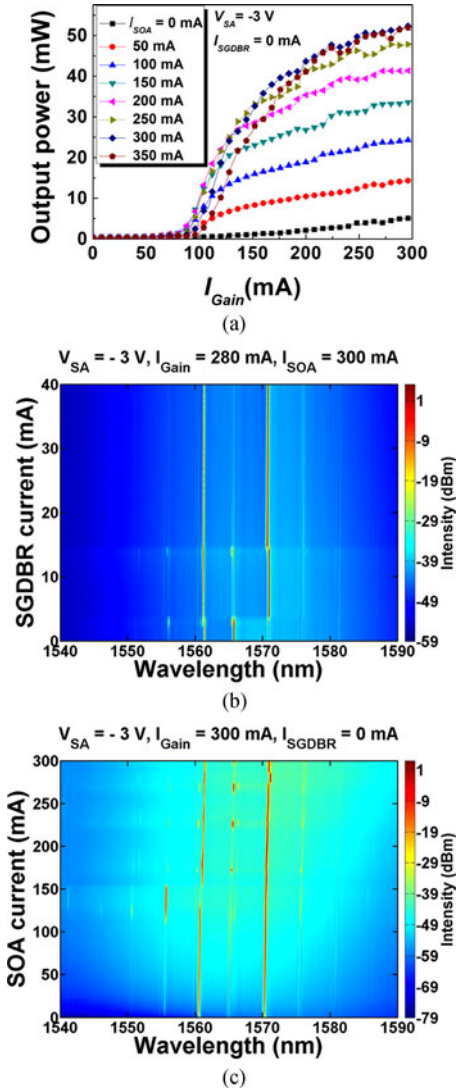

Fig. 4. (a) Typical output power from the SOA side as a function of the gain current with different I_{SOA} (from 0 mA to 350 mA with steps of 50 mA) when the $V_{SA} = -3$ V and $I_{SGDBR} = 0$ mA; 2D optical spectra as a function of (b) I_{SGDBR} and (c) I_{SOA}.

Passive mode-locking of the device was obtained by forward biasing the gain, SGDBR, and SOA sections and reverse biasing the SA section.

Fig. 4(a) shows the average output power (measured from the SOA output facet) versus the gain current (I_{Gain}) for different SOA currents (I_{SOA}) with an applied SA reverse voltage (V_{SA}) of -3 V and SGDBR current (I_{SGDBR}) of 0 mA. The threshold current was 70 mA. The waveguide loss in the C-SGDBR section includes internal loss, saturation absorption, and scattering loss, altogether totaling $\sim 20\,\text{cm}^{-1}$. An average output power of 52 mW was achieved at $I_{\text{Gain}} = 300$ mA, $I_{SOA} = 300$ mA, beyond which the SOA saturated. Kinks were observed on some of the *L–I* curves. These are typical for a DBR laser, being caused by thermal detuning between the gain, SGDBR, and SOA sections, and are associated with the observed mode hopping phenomenon [13]. Fig. 4(b) shows the 2D optical spectra for a range of I_{SGDBR} from 0 mA to 40 mA when $V_{\text{SA}} = -3$ V,

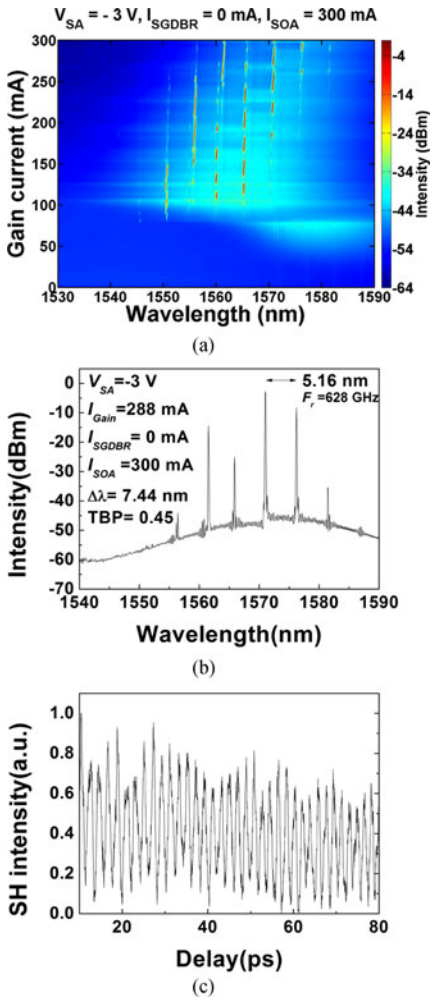

Fig. 5. The performance of C-SGDBR MLLD integrated with an SOA under the operation conditions of $V_{SA} = -3$ V, $I_{SGDBR} = 0$ mA, $I_{SOA} = 300$ mA: (a) 2D optical spectra as a function of gain current, (b) optical spectrum at the point of $I_{\rm Gain} = 288$ mA, (c) corresponding AC showing mode-locking F_r of 628 GHz.

$I_{\rm Gain} = 280$ mA, and $I_{SOA} = 300$ mA. Fig. 4(c) shows the longitudinal mode spacing was independent of $I_{SOA,}$ although the channel peaks were slightly influenced by thermal tuning, as evidenced by the small red shift. The absence of Fabry-Perot features confirms that reflections from the SOA output side can be neglected. The results also confirm that $\lambda_{\rm peak}$ and the mode spacing are accurately determined by Λ and P respectively. The longitudinal mode spacing is essentially independent of I_{SGDBR} and temperature.

Stable mode-locking over a wide range of drive parameters is an important feature for these MLLDs as it simplifies the operation for end-users. Pure mode-locked operation at ~640 GHz pulse repetition frequency was observed for a large range of laser bias parameters: $I_{\rm Gain}$ varied from 40 mA to 290 mA, V_{SA} from 0 V to −3.0 V, I_{DBR} from 0 mA to 20 mA (below the threshold current of the SGDBR section), and I_{SOA} from 0 mA to >300 mA.

Fig. 5(a) shows the 2D optical spectra for a range of $I_{\rm Gain}$ from 0 mA to 300 mA when $V_{\rm SA} = -3.0$ V, $I_{SGDBR} = 0$ mA and $I_{SOA} = 300$ mA. The spectrum was measured with a resolution bandwidth of 0.07 nm. The laser shows stable operation with a mode spacing of around 5.16 nm. As $I_{\rm Gain}$ was increased, the peak wavelength red-shifted. The optical spectrum with $I_{\rm Gain} = 288$ mA is shown in Fig. 5(b). The central wavelength is 1570 nm with a channel average spacing of 5.16 nm and a 3 dB bandwidth of 7.44 nm. This spacing of the peak wavelength between adjacent channels is less than the designed value of 5.22 nm, but the apparent error is within the resolution bandwidth of the optical spectrum analyzer of 0.07 nm. The main peak wavelengths of adjacent channels in Fig. 5(b) are not perfectly equidistant, which we ascribe to the large dispersion of the gratings ($dn/d\lambda = -2.1 \times 10^{-4}$ nm^{-1}). The average channel spacing corresponds to an F_r of ~628 GHz. The measured AC trace is shown in Fig. 5(c), under the following bias conditions: $V_{SA} = -3.0$ V, $I_{\rm Gain} = 288$ mA, $I_{SGDBR} = 0$ mA, and $I_{SOA} = 300$ mA. The average period of the measured emitted pulse train was 1.59 ps, which corresponds to an F_r of 628 GHz, in accordance with the optical spectrum mode spacing shown in Fig. 5(b). The AC width of an isolated pulse was 0.77 ps, which deconvolves to a pulse width of 0.50 ps, assuming a sech^2 pulse shape. The time-bandwidth product (TBP) of the pulse is equal to 0.45, which is somewhat larger than the transform-limit (≈0.315) for a sech^2 pulse shape, due to self-phase modulation (SPM) in the gain and SOA sections [14]. The average output power was 51.5 mW, and the corresponding peak power was 142 mW.

Although the second harmonic frequency of $F_r \sim 1.20$ THz is visible when $I_{\rm Gain} < 294$ mA and $|V_{SA}| > 2.4$ V, the most obvious area of second harmonic operation area is with $I_{\rm Gain} \geq 294$ mA and $|V_{SA}| \leq 2.4$ V. We favor the suggestion that the effect occurs as a result of the presence of two high intensity pulses propagating in each of the DBR sampled grating sections simultaneously, which overlap and interfere in the middle of the sections.

Fig. 6(a) shows the 2D optical spectra for a range of $I_{\rm Gain}$ values from 0 mA to 300 mA when $V_{SA} = -2.4$ V and $I_{SGDBR} = 0$ mA. An evolution to mode-locking at the 2nd harmonic can be observed when $I_{\rm Gain}$ is between 294 mA and 300 mA. The optical spectrum at $I_{\rm Gain} = 300$ mA is shown in Fig. 6(b), where the central wavelength is 1567 nm with a channel spacing of 9.6 nm and 3 dB bandwidth of 9.53 nm. The spacing of the peak wavelength of the adjacent channel is nearly double that shown in Fig. 5(b). The measured AC trace is shown in Fig. 6(c) where the average period of the measured emitted pulse train is 0.83 ps, which corresponds to an F_r of 1.20 THz (approximately the 2nd harmonic). The AC width of an isolated pulse was 0.43 ps, which deconvolves to a pulse width of 0.28 ps, assuming a sech^2 pulse shape. The TBP of the pulse is equal to 0.33, which is nearly transform-limited (≈0.315) for a sech^2 pulse shape. The average output power was 54.4 mW and the corresponding peak power was 142 mW.

V. PPS-SGDBR MLLD Integrated With an SOA

We now consider the use of π-phase steps within the sampling period to increase the coupling. To confirm that the

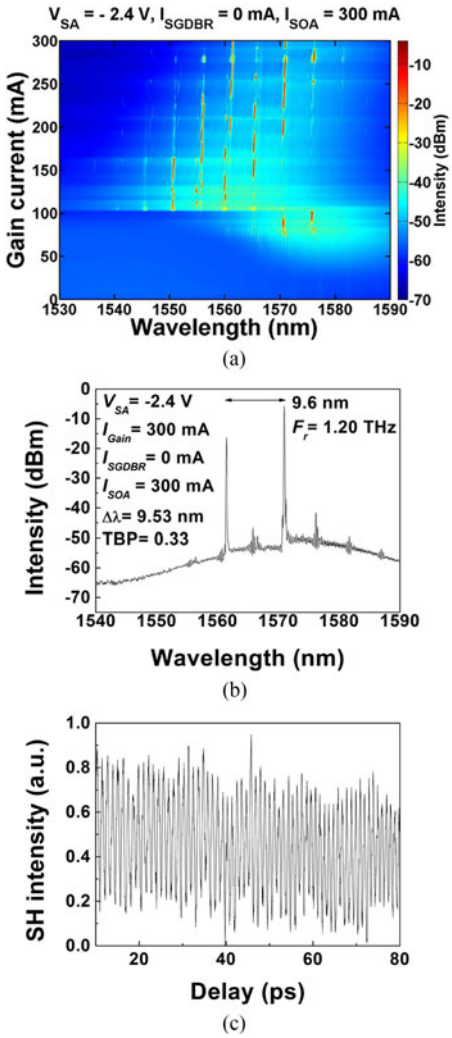

Fig. 6. The performance of C-SGDBR MLLD integrated with an SOA under the operation conditions of $V_{SA} = -2.4$ V, $I_{SGDBR} = 0$ mA, $I_{SOA} = 300$ mA: (a) 2D optical spectra as a function of gain current, (b) optical spectrum at the point of $I_{\mathrm{Gain}} = 300$ mA, (c) corresponding AC traces showing mode-locking F_r of 1.20 THz.

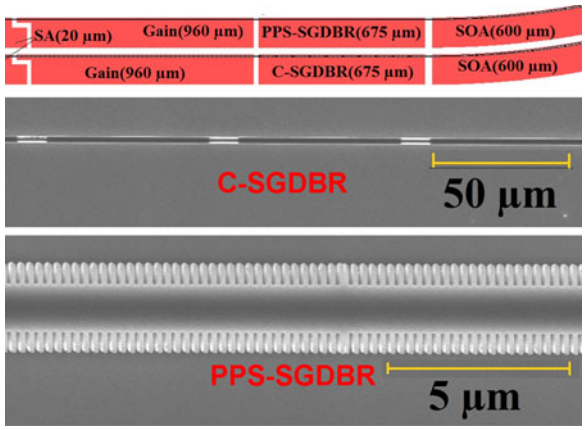

Fig. 7. Device structures based on C-SGDBR and PPS-SGDBR and their SEM pictures.

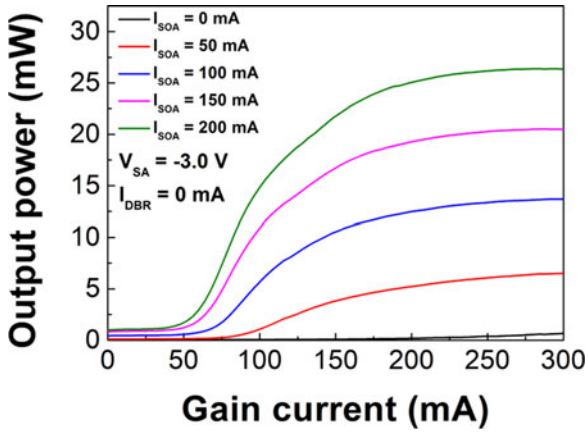

Fig. 8. Typical output power from the SOA side of the PPS-SGBBR laser vs the gain current with different I_{SOA} (from 0 mA to 200 mA with steps of 50 mA) when the $V_{SA} = -3$ V and $I_{PPS-SGDBR} = 10$ mA.

PPS-SGDBRs have an increased effective κ, we fabricated sub-THz repetition frequency MLLDs monolithically integrated with SOAs based on the configurations of C-SGDBR and PPS-SGDBR described in Fig. 2(a) and Fig. 2(b) respectively. The 0^{th} order gratings have a period (Λ) of 246 nm, sampling period $P = 67.5\,\mu$m, and the grating burst $P_1 = 10\,\mu$m and 17 μm for the C-SGDBR and PPS-SGDBR respectively. To make a valid comparison possible, both types of device were fabricated close together, pair by pair, in the same bars. Devices based on the C-SGDBR and PPS-SGDBR and their SEM pictures are shown in Fig. 7. Compared with Fig. 3(a), the only differences for the C-SGDBR are that the SOA length is 600 μm instead of 550 μm, the grating period $\Lambda = 246$ nm, and the gap between the SOA and SGDBR sections is 30 μm instead of 50 μm.

Fig. 8 shows the average output power (from the SOA side) versus I_{Gain} for different I_{SOA} with an applied V_{SA} of -3 V and PPS-SGDBR current ($I_{PPS-SGDBR}$) of 10 mA for the case of the PPS-SGDBR MLLD. The threshold currents for all the I_{SOA} cases are less than 50 mA with a maximum average output power of 27.8 mW after the SOA. Although the PPS-SGDBR section loss is higher than that of the C-SGDBR due to the longer effective length of the PPS-SGDBR, its mirror reflectivity is much higher than that of the C-SGDBR, so the threshold current can be the same as or even lower than that of the C-SGDBR. The relatively lower output power may be due to two reasons: the higher mirror reflectivity resulting in a lower slope efficiency for the PPS-SGDBR, and a lower peak gain in the 600 μm long SOA because the peak gain of an SOA is inversely proportional to the SOA's active volume. The latter effect is likely to be dominant.

Fig. 9(a) shows the corresponding lasing spectra of both C-SGDBR and PPS-SSDBR MLLDs under operating conditions of $V_{SA} = -3$ V, $I_{\mathrm{Gain}} = 144$ mA, $I_{SGDBR} = 10$ mA, $I_{SOA} = 150$ mA. As we pointed out in Section II, for these devices, the uniform grating $\kappa_0 \approx 23.2\,\mathrm{cm}^{-1}$, much lower than the value of $80\,\mathrm{cm}^{-1}$ in the C-SGDBR MLLDs integrated with an SOA reported in Section IV. However, the effective κ of the PPS-SBG is significantly larger than that of the C-SGDBR,

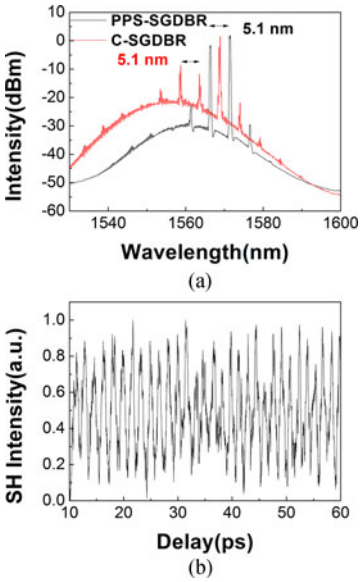

Fig. 9. (a) The optical spectra of C-SGDBR and PPS-SGDBR MLLDs measured at $V_{SA} = -3$ V, $I_{\mathrm{Gain}} = 144$ mA, $I_{SGDBR} = 10$ mA, $I_{SOA} = 150$ mA and (b) measured autocorrelation trace for PPS-SGDBR.

giving a clearer and sharper reflection comb with a wavelength spacing of 5.1 nm. For the same reason, the amplified spontaneous emission (ASE) level of the PPS-SGDBR MLLD output spectra is much lower than that of the C-SGDBR MLLD. The central wavelength was 1569.2 nm with a 3 dB bandwidth of 6.54 nm. The measured autocorrelation trace of the PPS-based devices is shown in Fig. 9(b). Because the gain peak is red-shifted by 10 nm, the number of longitudinal modes is reduced and the AC trace is noisier than that in Fig. 5(c). The average period of the pulse train is 1.6 ps, corresponding to an F_r of 620 GHz, and the pulse width is 0.54 ps. The average output power is 19 mW, with a corresponding peak power of about 50 mW.

The PPS-SGDBR has the same characteristics as that of C-SGDBR, i.e., λ_{peak} and the mode spacing are accurately determined by Λ and P respectively. The longitudinal mode spacing is essentially independent of I_{SGDBR} and temperature.

Recently we have fabricated PPS-SGDBR lasers with a still higher F_r – namely 1 THz – taking mode-locked operation well into the ITU defined THz frequency band (275 GHz to 3 THz).

The device configuration is similar to the PPS-SGDBR integrated with an SOA shown in Fig. 7. The only difference is the PPS-SGDBR section is 648 μm long and the 0^{th} order grating period $\Lambda = 244$ nm. The duty cycle of the PPS-SGDBR is still chosen to be $P_1/P = 0.25$, $P = 43.2\,\mu$m, $P_1 = 11\,\mu$m, $N_s = 15$. The effective κ of the PPS-SGDBR is expected to be around twice $((43.2 - 2 \times 11)/11 = 1.93)$ that of a C-SGDBR and nearly half $((43.2 - 2 \times 11)/43.2 = 0.49)$ that of a uniform grating. Transfer matrix simulations of the reflectivity of the PPS-SGDBR and a comparison with the corresponding C-SGDBRs are shown in Fig. 10(a), which confirms the above analysis. The central peak wavelength (λ_{peak}) is 1560.5 nm and the spacing between reflectivity peaks is about 8.1 nm.

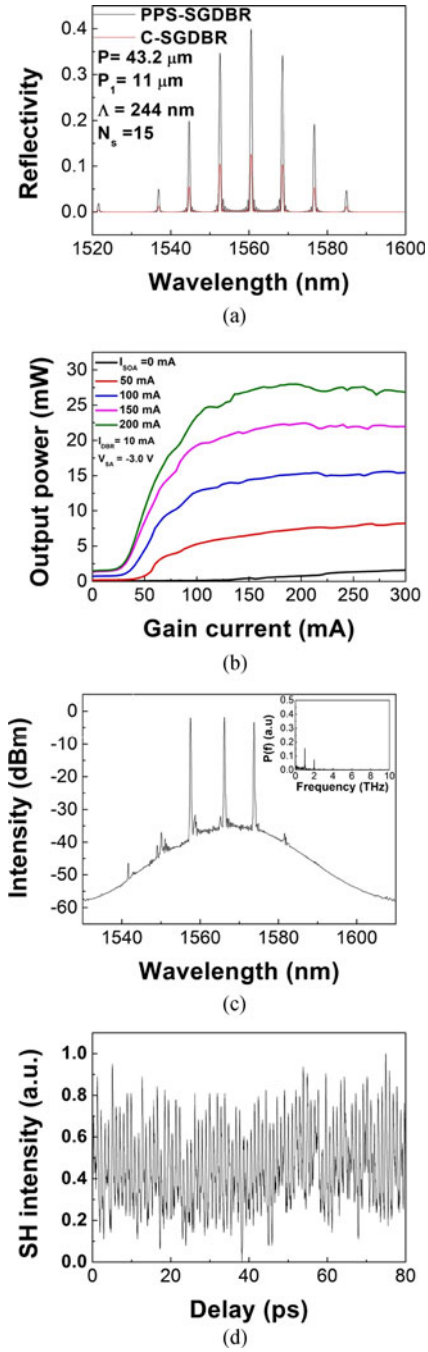

Fig. 10. (a) Simulated reflectivity spectra of the 1THz PPS-SGDBR and its counterpart C-SGDBR, (b) typical output power from the SOA side vs the gain current with different I_{SOA} (from 0 mA to 200 mA with steps of 50 mA) when the $V_{SA} = -3$ V and $I_{PPS-SGDBR} = 10$ mA, (c) the optical spectrum and FFT of AC trace(inset) measured at $V_{SA} = -3$ V, $I_{\mathrm{Gain}} = 232$ mA, $I_{PPS-SGDBR} = 10$ mA, $I_{SOA} = 100$ mA and (d) measured autocorrelation trace for the PPS-SGDBR.

Fig. 10(b) shows the average output power versus the gain I_{Gain} for different I_{SOA} with an applied V_{SA} of -3 V and $I_{PPS-SGDBR}$ of 10 mA for a PPS-SGDBR laser mode-locked at 1 THz. A maximum output power of 28 mW was achieved which is nearly the same as that in Fig. 8 for the 620 GHz PPS-SGDBR device.

In our devices, although the uniform grating $\kappa_0 \approx 23.2\,\mathrm{cm}^{-1}$ because of the RIE lag effect, the effective κ of the PPS-SGDBR is nearly twice of that of the counterpart C-SGDBR. As can be seen in Fig. 10(c), the reflection comb is clearer and sharper than that of the C-SGDBR with an average wavelength spacing of around 8.1 nm, the same as the simulation results in Fig. 10(a). Again, the main peak wavelengths of adjacent channels in Fig. 10(c) are not perfectly equidistant, which we ascribe to the large dispersion of the gratings ($dn/d\lambda = -2.1 \times 10^{-4}$ nm^{-1}). The central wavelength is 1564.5 nm with a 3 dB bandwidth of 9.14 nm. Fig. 10(d) shows the corresponding autocorrelation traces, with the bias conditions indicated in the caption. The average period of the pulse train was measured to be 1.0 ps, corresponding to an F_r of 1 THz. The fast Fourier transform (FFT) of the AC trace is plotted inset in Fig. 10(c) which shows both fundamental mode-locked frequency at 1 THz and its higher harmonics. This leads to the irregularities in the AC trace. The AC width of an isolated pulse was 0.59 ps, which deconvolves to a pulse width of 0.38 ps, assuming a sech^2 pulse shape. The TBP of the pulse is equal to 0.43, higher than the transform-limited value ($\approx$0.315) for a sech^2 pulse shape. This means the pulse signal has a significant chirp which is again attributed to SPM in the laser gain and SOA sections [14]. The average output power was 15 mW with a corresponding peak power of about 35 mW.

VI. Conclusion

In conclusion, by integrating an SOA, we have increased the output power of 1.5 μm range AlGaInAs/InP MLLDs operating at both 628 GHz and a second harmonic of 1.20 THz. After the SOA, the peak power of the pulses is as large as 142 mW. Fundamental operation of MLLDs at $F_r = 620\,\mathrm{GHz}$ and $F_r = 1\,\mathrm{THz}$ has also been successfully demonstrated, based on PPS-SGDBRs. Compared with C-SGDBRs, PPS-SGDBRs increase the effective coupling coefficient and the optical phase is managed along the entire length of the grating, resulting in cleaner and sharper optical spectra with a much lower level of ASE. Compared with other reported devices, our lasers based on side-wall etched SGDBRs use simple and reproducible fabrication technologies and exhibit highly controllable and robust mode-locked operation. These high power MLLDs are expected to be used as pumping source to produce the THz signal when using the photomixing techniques.

Acknowledgment

The authors would like to thank the staff of the James Watt Nanofabrication Centre, University of Glasgow, for help in fabricating the devices.

References

[1] S. Arahira, Y. Matsui, and Y. Ogawa, "Mode-locking at very high repetition rates more than terahertz in passively mode-locked distributed-Bragg-reflector laser diodes," *IEEE J. Quantum Electron.*, vol. 32, no. 7, pp. 1211–1224, Jul. 1996.

[2] D. A. Yanson *et al.*, "Ultrafast harmonic mode-locking of monolithic compound-cavity laser diodes incorporating photonic-bandgap reflectors," *IEEE J. Quantum Electron.*, vol. 38, no.1, pp. 1–11, Jan. 2002.

[3] T. Shimizu, I. Ogura, and H. Yokoyama, "860 GHz rate asymmetric colliding pulse mode locked diode lasers," *Electron. Lett.*, vol. 33, no. 22, pp. 1868–1869, 1997.

[4] J. H. Marsh and L. Hou, "Mode-locked laser diodes and their monolithic integration," *IEEE J. Sel. Top. Quantum Electron.*, vol. 23, no. 6, Nov./Dec. 2017, Art. no. 1100611

[5] L. Hou, M. Haji, and J. H. Marsh, "Mode locking at terahertz frequencies using a distributed Bragg reflector laser with a sampled grating," *Opt. Lett.*, vol. 38, pp. 1113–1115, 2013.

[6] S. Tang, L. Hou, X. Chen, and J. H. Marsh, "Multiple-wavelength distributed-feedback laser arrays with high coupling coefficients and precise channel spacing," *Opt. Lett.*, vol. 42, no. 9, pp. 1800–1803, 2017.

[7] M. Tani, P. Gu, M. Hyodo, K. Sakai, and T. Hidaka, "Generation of coherent terahertz radiation by photomixing of dual-mode lasers," *Opt. Quantum Electron.*, vol. 32, no. 4, pp. 503–520, 2000.

[8] L. Hou *et al.*, "Subpicosecond pulse generation at quasi-40-GHz using a passively mode locked AlGaInAs/InP 1.55 μm strained quantum well laser," *IEEE Photon. Technol. Lett.*, vol. 21, no. 23, pp. 1731–1733, Dec. 2009.

[9] L. Hou *et al.*, "Monolithic 40-GHz Passively Mode-Locked AlGaInAs–InP 1.55- μm m MQW Laser With Surface-Etched Distributed Bragg Reflector," *IEEE Photon. Technol. Lett.*, vol. 22, no. 20, pp. 1503–1505, Oct. 2010.

[10] L. Hou, M. Haji, and J. H. Marsh, "Monolithic mode-locked laser with an integrated optical amplifier for low-noise and high-power operation," *IEEE J. Sel. Topics Quantum Electron.*, vol. 19, no. 4, Jul./Aug. 2013, Art. no. 1100808.

[11] A. J. Collar *et al.*, "Low residual reflectivity of angled-facet semiconductor laser amplifiers," *IEEE Photon. Technol. Lett.*, vol. 2, no. 8, pp. 553–555, Aug. 1990.

[12] T. Nakura and Y. Nakano, "LAPAREX-An automatic parameter extraction program for gain-and index-coupled distributed feedback semiconductor lasers, and its application to observation of changing coupling coefficients with currents," *IEICE Trans. Electron.*, vol. 83, pp. 488–495, 2000.

[13] J. Fricke, H. Wenzel, M. Matalla, A. Klehr, and G. Erbert, "980-nm DBR lasers using higher order gratings defined by i-line lithography," *Semicond. Sci. Technol.*, vol. 20, pp. 1149–1152, 2005.

[14] G. P. Agrawal and N. A. Olsson, "Self-phase modulation and spectral broadening of optical pulses in semiconductor laser amplifier," *IEEE J. Quantum Electron*. vol. 25, no. 11, pp. 2297–2306, Nov. 1989.

Lianping Hou (M'11) received the B.Eng. degree from the Central-South University of Technology, Changsha, China, in 1992, the M.A. degree from Huazhong University of Science and Technology, Wuhan, China, in 2003, and the Ph.D. degree from the Chinese Academy of Sciences, Beijing, China, in 2005.

In 2006, he was with the Department of Electrical and Electronic Engineering, University of Bristol, as a Research Associate, working on a European Commission FP6-IST Project involved with multifunctional integrated arrays of interferometer switches. In 2007, he was with the School of Engineering, University of Glasgow, as a Research Associate, where he worked on developing high-frequency and high-power semiconductor mode-locked lasers. In 2012, he was promoted to Research Fellow. He is currently a Lecturer with the University of Glasgow, Glasgow, U.K., working on nanofabrication, semiconductor laser technology, and integrated optics. He is the author and coauthor of more than 120 papers and the inventor of several patents. He is a member of the Optical Society of America.

Song Tang received the B.S. and M.E. degrees from Nanjing University, Nanjing, China, in 2012 and 2015, respectively. He is currently working toward the Ph.D. degree at the University of Glasgow, Glasgow, U.K. He is the author and coauthor of several journal papers and conference papers and the inventor of several patents.

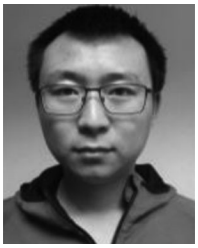

Bin Hou received the double Bachelor's degree of science from Jilin University, Changchun, China, and Tomsk Polytechnic University, Tomsk, Russia, in 2014, and Master's degree of science from Moscow State University, Moscow, Russia, in 2017. He is currently working toward the Ph.D. degree in the School of Engineering, University of Glasgow, Glasgow, U.K., working on low-noise optically controlled terahertz-phased array antenna systems and integrated optics.

Song Liang was born in Liaoning, China. He received the B.S. and M.S. degrees from the Department of Material Physics, Beijing University of Science and Technology, Beijing, China, in 1999 and 2002, respectively, and the Ph.D. degree from the Institute of Semiconductors, Chinese Academy of Sciences, Beijing, China, in 2006. He is currently working as a Professor with the Institute of Semiconductor, Chinese Academy of Sciences. His current research includes the MOCVD growth of semiconductor materials and the fabrication of optoelectronics devices.

John H. Marsh (M'91–SM'91–F'00) received the B.A. degree from the Universities of Cambridge, Cambridge, U.K., the M.Eng. degree from the University of Liverpool, Liverpool, U.K., and the Ph.D. degree from the University of Sheffield, Sheffield, U.K. He is currently a Professor of optoelectronic systems with the University of Glasgow, Glasgow, U.K. He is currently the Dean with the University of Glasgow UESTC. His experience of semiconductor laser technology and integrated optics ranges from epitaxial growth through to the design and development of integrated laser modules for applications including advanced printing and imaging. He co-founded Intense Ltd. in 2000. His research interests include fundamental electrical and optical properties of semiconductors, development of novel optoelectronic devices, processes for creating photonic integrated circuits, integrated mode-locked lasers for ultrashort pulse generation, and the development and manufacturing of high-power laser array products.

He is a Fellow of Royal Academy of Engineering, Royal Society of Edinburgh, OSA, IET, Institute of Physics, and Royal Society of Arts. He was the recipient of the 2006 IEEE/LEOS Engineering Achievement Award with Catrina Bryce "for extensive development and commercialization of quantum well intermixing for photonic devices." He was also awarded the 2006 IEEE/LEOS Distinguished Service Award "for major contributions to LEOS governance and for leadership in promoting the development of LEOS as a global society." He was the President of the IEEE Photonics Society in 2008 and 2009. He is a Visiting Professor with the Queen's University Belfast and North West University, Xi'an, China.